

Applying Electrical Resistivity Tomography to the Identification of Endokarstic Geometries in the Pleistocene Sites of the Sierra de Atapuerca (Burgos, Spain)

A.I. ORTEGA^{1,2*}, A. BENITO-CALVO¹, J. PORRES³,
A. PÉREZ-GONZÁLEZ¹ AND M.A. MARTÍN MERINO²

¹ Centro Nacional de Investigación sobre Evolución Humana (CENIEH). Paseo Sierra de Atapuerca, 09002 Burgos, Spain

² Grupo Espeleológico Edelweiss. Excma. Diputación Provincial de Burgos. Paseo del Espolón s/n. 09071 Burgos, Spain

³ Área de Ingeniería del Terreno. Dpto. de Construcciones Arquitectónicas e I.C.T. Escuela Politécnica Superior. Universidad de Burgos, 09001 Burgos, Spain

ABSTRACT In this paper we have applied the electrical resistivity tomography (ERT) in order to prospect and to analyse the morphological and geological subsurface of the Torcas-Cueva Mayor endokarst system (Sierra de Atapuerca). These works are essential to establish the development of the sedimentary infills where the Early and Middle Pleistocene archaeo-palaeoanthropological sites of the Sierra de Atapuerca are located. The prospecting was based on the elaboration of 15 ERT sections, which were interpreted using topographic, archaeological, geological and geomorphological data. Through this procedure we have identified the endokarst morphologies and the main lithological groups. The latter correspond to the Upper Cretaceous limestones and dolostones ($> 1500 \text{ ohm m}^{-1}$) and Neogene sediments and Quaternary valley infills ($< 400 \text{ ohm m}^{-1}$). The endokarst structures inside the Upper Cretaceous carbonates were related to empty cavities ($> 1500 \text{ ohm m}^{-1}$), passages filled with speleothems ($400\text{--}1500 \text{ ohm m}^{-1}$) and with detrital materials ($< 400 \text{ ohm m}^{-1}$), such as the deposits of the Dolina, Elefante and Galería sites. The analysis of these subsurface structures shows that the karstic passages present a regular south–north development, starting with subsurface faults detected in the north margin of the main valley (Arlanzón River) and finishing along the Pico valley headwaters. These passages were cut off by the Pleistocene incision of the Sierra de Atapuerca minor valleys (e.g. Propiedad valley), forming entrances to caves that were occupied by hominids and fauna from Early Pleistocene times. Copyright © 2010 John Wiley & Sons, Ltd.

Key words: Electrical resistivity tomography; cave; geoarchaeological prospecting; Sierra de Atapuerca sites; Schlumberger–Wenner geoelectric; dipole–dipole geoelectric

Introduction

Geoelectrical prospecting has been used extensively in geophysical investigation for many years, and has been applied to hydrological studies, mining and geotechnical research (Griffiths and Barker, 1993; Maillol *et al.*, 1999; Daily and Ramirez, 2000; Dahlin, 2001). More recently, it has been used in environmental

studies and in archaeology (Griffiths and Barker, 1994; Piro *et al.*, 2000, 2001; Chambers *et al.*, 2002; Papadopoulos *et al.*, 2006, 2010; Astin *et al.*, 2007; Drahor *et al.*, 2008; Cardarelli and Di Filippo, 2009; Tsokas *et al.*, 2009), providing interesting information about the site geometry, including those areas not excavated. The application of electrical resistivity tomography (ERT) for imaging of subsurface discontinuities and lithological contacts is well documented (Beresnev *et al.*, 2002). Electrical resistivity tomography constitutes an important advance in the geoelectric methods because it solves automatically the manual

* Correspondence to: A.I. Ortega, Centro Nacional de Investigación sobre Evolución Humana (CENIEH). Paseo Sierra de Atapuerca, 09002 Burgos, Spain. E-mail: anaisabel.ortega@eb.cenieh.es

change of electrodes, characteristic of the classic geoelectrical methods (vertical electrical sounding). In this way, ERT facilitates the management and fast processing of a large number of data, constituting a useful non-destructive method to detect subsurface structures.

We have applied ERT to the prospection of endokarst morphologies and the sedimentary infills of the Torcas-Cueva Mayor endokarst system (Eraso *et al.*, 2001; Ortega *et al.*, 2005; Ortega, 2009), where the Early and Middle Pleistocene Sierra de Atapuerca archaeo-palaeoanthropological sites are located (Arsuaga *et al.*, 1993, 1997; Bermúdez de Castro *et al.*, 1997, 1999, Carbonell *et al.*, 1999, 2008). The goal of this prospection was to solve some key aspects of the geodynamic evolution of this endokarst system, such as: (i) the determination of the depth of the geological contacts and structures that control the development of the endokarst; (ii) the analysis of the endokarstic morphologies (passage continuities and geometries); and (iii) the detection and spatial distribution of the sedimentary infills. The last point constitutes basic information to understanding the formation of the known archaeological sites and provides new information about potential areas for investigation, such as filled old entrances. For this purpose, ERT profiles were focused on the bedrock structures in southwest Sierra de Atapuerca minor valleys (Propiedad, Valhondo and Cueva Mayor), which divide the distribution of the endokarst system and are associated with the formation of the Elefante, Dolina and Galería sites.

Geological and geomorphological background

The Sierra de Atapuerca is located in the northeast area of the Cenozoic Duero Basin (north-central Iberian Peninsula, Figure 1A), which connects with the Ebro Basin through the Bureba Corridor. Toward the north and southeast the northeast Duero Basin is delimited by the Iberian and Cantabrian Ranges formed by the Alpine orogeny (Figure 1A and B). In this framework, the Sierra de Atapuerca forms a *mont*, composed of Mesozoic sediments folded during the Alpine orogeny as part of a NNW–SSE overturned anticline, faulted at its northern end (Pineda, 1997; Benito, 2004). In the south of the Sierra de Atapuerca, Turonian to Lower Santonian marine limestones and dolostones crop out, in which develop the Sierra de Atapuerca endokarst system (Martín *et al.*, 1981; Ortega, 2009). These Upper Cretaceous carbonates are buried by endorrheic continental Cenozoic sediments (Figure 1B), associated

with the development of erosion surfaces in the Sierra de Atapuerca (Benito-Calvo and Pérez-González, 2007). The Cenozoic deposits comprise syntectonic conglomerates and clays (Oligocene to Lower Miocene), and a post-orogenic Neogene sequence (Armenteros *et al.*, 2002). In the study area, the latter comprises alluvial and lacustrine sediments, where three units separated by discontinuities can be distinguished (Benito-Calvo and Pérez-González, 2007), from the Lower Miocene (Orleanian) to the Upper Miocene (Vallesian).

At the end of the Neogene endorrheic infill (Upper Miocene to Pliocene), the Duero Basin was opened to the Atlantic Ocean, starting the formation and incision of the Quaternary fluvial network, represented in the study area by Arlanzón River and its main tributaries, the Vena and Pico Rivers (Figure 1B). The Quaternary evolution of these valleys is characterized by several stages of incision and aggradation, leaving a fluvial sequence of 14 fluvial terraces and the current floodplain (Benito, 2004). Magnetostratigraphic data locates terrace T4 (+60–67 m), with a reversed magnetic polarity, as well as older terraces in the Early Pleistocene (Benito-Calvo *et al.*, 2008). Thermoluminescence dating conducted on the lower terraces (Benito-Calvo *et al.*, 2008) associate T11 (+12–13 m) with the Middle–Upper Pleistocene boundary (115 052 ± 11 934 yr BP) and T14 (+2–3 m) with the Holocene (4827 ± 338 yr BP).

The geomorphological evolution of these base levels during the Neogene and Pleistocene has controlled the formation of the Sierra de Atapuerca minor valleys (Benito-Calvo *et al.*, 2008), besides the onset and development of the Torcas-Cueva Mayor endokarst. This presents medium mountain characteristics, being characterized by a multilevel system concentrated in the northwest margin of the Sierra de Atapuerca (San Vicente Unit). The karstic levels comprise paragenetic passages formed in active regimes associated with the phreatic levels developed during the stability of the base levels (water-table cave; Ford, 1977). At present, this system is defined by three inactive horizontal levels situated at +90, +70 and +60 m with respect to the Arlanzón River. The passages show a progressive migration to the west, from the upper oldest level to the lower youngest level, and are connected by pits and chambers.

The first level is composed of phreatic paragenetic passages developed at 1015–1020 m a.s.l. (Galería del Sílex-Salón del Coro-Galería de las Estatuas; Figure 1C). The second level (Sala de los Cíclopes-Galería del Silo-Galería Baja-Elefante and Dolina-Galería Complex infills; Figure 1C), is characterized

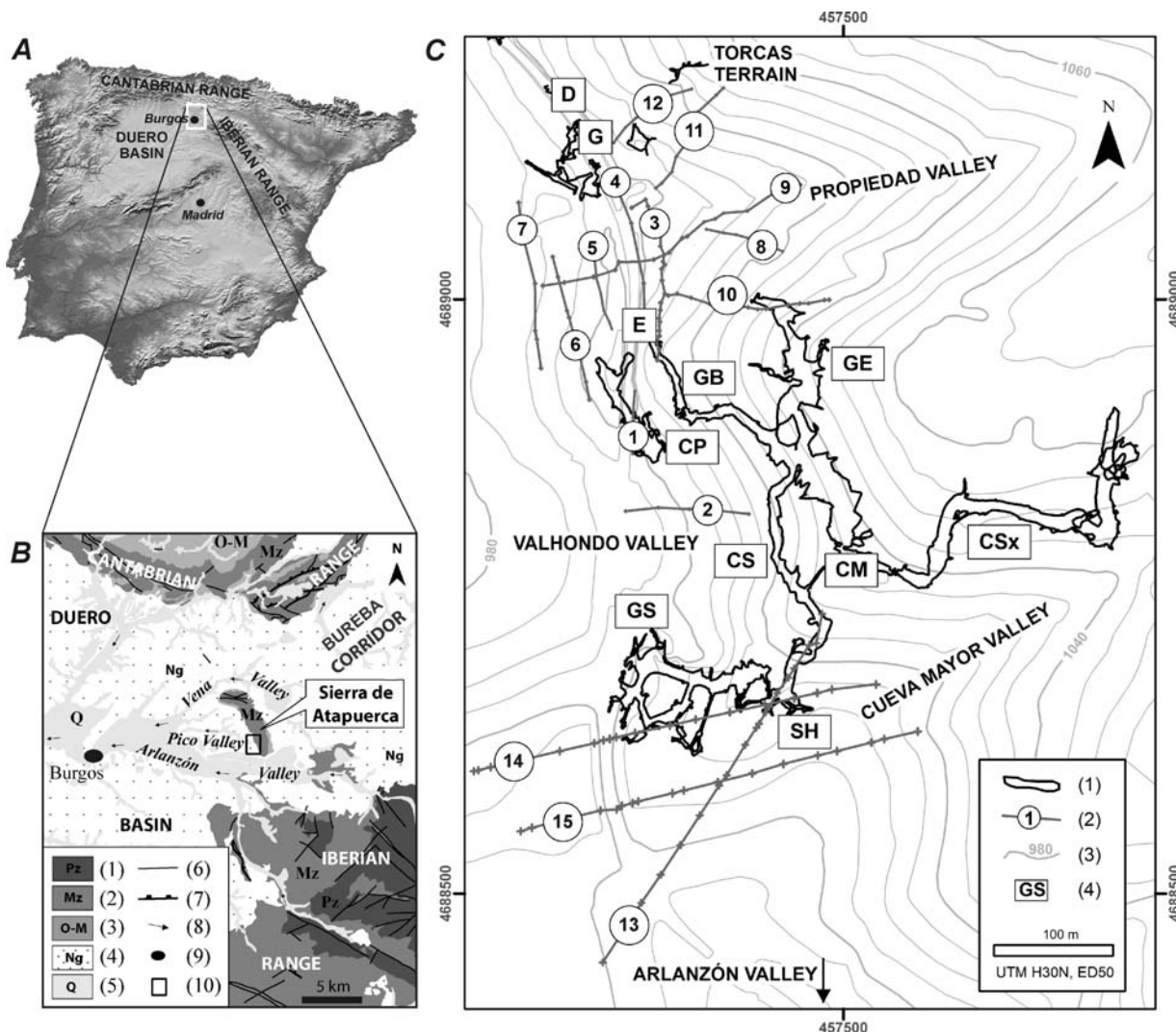


Figure 1. (A) General location of the study area in the Iberian Peninsula. (B) Geological map of the northwest Duero Basin. Legend: 1, Palaeozoic; 2, Mesozoic; 3, Oligocene–Lower Miocene; 4, Neogene; 5, Quaternary; 6, fault; 7, thrust; 8, drainage direction; 9, city; 10, study area in Figure 1C. (C) Distribution of the geoelectrical profiles recorded in the southern flank of the Sierra de Atapuerca. Legend: 1, map of the endokarst system; 2, electrical resistivity tomography profiles; 3, topographic contours in metres (Junta de Castilla y León); 4, passage names: D, Dolina; G, Galería; E, Elefante; GB, Galería Baja; GE, Galería de las Estatuas; CP, Cueva Peluda; GS, Galería del Silo; CS, Cueva del Silo; CM, Cueva Mayor; CSx, Cueva del Sílex; SH, Sima de los Huesos.

by horizontal passages at 1000–1005 m a.s.l. (Ortega, 2009). Some of these passages became vadose zones during the Early Pleistocene, being opened and allowing allochthonous infills where the Elefante, Dolina and Galería sites developed (Parés and Pérez-González, 1995; Pérez-González *et al.*, 2001; Parés *et al.*, 2006). The third level presents less extension, being composed of a rectangular network of passages, according to the rock fracture pattern (Palmer, 1991). This network is organized from a main axis that drains toward the northwest where the old spring would have been located. This level developed at 995–985 m a.s.l. (Sima de los Huesos–Cueva del Silo–Cueva Peluda

and Cueva del Compressor; Figure 1C), and contains fluvial deposits derived from the Arlanzón River (Ortega *et al.*, 2005). The genesis of these levels has been related to a hypogenetic origin, where water comes from a confined aquifer following the tectonic structures (Klimchouk, 2009; Ortega, 2009).

Methodology

Geophysical methods constitute a useful tool to obtain basic information about the site setting, which can be applied to plan new excavations and to understand

the use of the space (Benech and Hesse, 2007). Among the different geophysical methods, electrical resistivity tomography (ERT) is frequently used in archaeology and karstic investigations, since it is a low cost method suitable to estimate the depth and geometry of structures.

Electrical resistivity tomography consists of the spatial distribution analysis of the subsurface electric resistivity. This analysis is carried out through a large number of measurements recorded from the terrain surface or from boreholes. Electrical resistivity tomography is based on the implantation of a large number of electrodes with an equidistant gap (Griffiths *et al.*, 1990), generally along a straight longitudinal profile, although other geometries, such as grids and lines at an angle are also possible. The gap between electrodes determines the resolution and depth of the prospecting (small gap, high resolution and low depth, and *vice versa*). These electrodes are connected simultaneously to the resistivity device, which controls which electrodes are active and their configuration, thanks to a sequential program specific for every job (Porres, 2003). The geometry of the electrodes defines the array, and this can be varied although the most common are Schlumberger–Wenner and dipole–dipole arrays (Beresnev *et al.*, 2002).

The aim of these techniques is to determine the real electric resistivity value and its spatial distribution, using the apparent resistivity values obtained by means of conventional direct current methods. Then, the data are processed applying algorithms which estimate a theoretical model from the measured section (Loke and Barker, 1996; Loke and Dahlin, 2002; Porres, 2003). The apparent resistivity pseudo-section taken in the field is subjected to an inversion process, from which a distance–depth section is obtained. This section shows the continuous distribution of the terrain resistivity, expressed by a colour scale. The variations in the resistivity values recorded in the section are related to subsurface characteristics and structures, and consequently can be interpreted geologically (lithology, contacts, fractures, faults, water, cavities, etc). Combining the lateral resolution and the length, ERT constitutes an effective method to scan the subsurface in a wide range of depths, independent of the terrain topography.

In order to interpret the resistivity sections correctly, the interrelation between the several key factors that control terrain resistivity must be considered, such as lithology (especially clays), porosity, water saturation and temperature, or salinity. In addition, different geological configurations may have a similar electric response (Porres, 2003). For these reasons, interpretation of the tomographic sections should be

supported by geological observations and control profiles. The latter must be carried out at known geological points, in order to obtain the resistivity behaviour of the underground materials and discontinuities, allowing the comparison with other sections.

Results

Electrical resistivity tomography prospecting was carried out in the southwest margin of the Sierra de Atapuerca, where cave entrances occupied by hominids during Pleistocene are located. The survey centred on the Valhondo, Propiedad and Cueva Mayor valleys, and in the Torcas Terrain (Figure 1C). The number, distribution and technical characteristics of the geophysical profiles are shown in the Table 1. The survey was carried out with the resistivity device SYSCAL R1 PLUS Switch72, and the data were processed using the software RES2DINV ver.3.42 (Loke, 1999). In every profile, we applied Schlumberger–Wenner and dipole–dipole electrode arrays. Most of the profiles present similar results for both the dipole–dipole and Schlumberger–Wenner arrays, although in a few profiles they differ substantially, especially in those where the prospecting depth is increased (Athanasidou *et al.*, 2007). In these cases, the dipole–dipole showed the highest root-mean-squared (RMS) errors (Table 1). Also the Schlumberger–Wenner profiles provide more realistic images according to the endokarstic and geological structures observed in the Cueva Peluda control profile (Figure 2), so we have based the geophysical interpretation mainly on the Schlumberger–Wenner array data. In order to facilitate comparison, the colour scale was standardized for all the profiles. In addition, the sections were drawn without vertical exaggeration, in order to facilitate georeferencing and projection of the karstic passage topography. The topography of the geophysical sections was elaborated from topographic surveys. Key profiles can be seen in Figures 2–6.

Interpretation and discussion

The geophysical interpretation of these sections was supported by archaeological and geological field observations using 1:50 000 and 1:10 000 geological and geomorphological surface maps (Pineda, 1997; Benito, 2004), and using the geomorphology of the known endokarst system, elaborated by detailed surveying (Ortega, 2009). In the same way, profile 1 (Figures 1C.1 and 2, and Table 1) was conducted

Table 1. Technical characteristics of the Electrical resistivity tomography sections carried out in the south flank of the Sierra de Atapuerca.

Section number	Distance (m)	Electrode spacing	Number of iterations	Root mean square (m)		Coordinates (UTM H30N, ED50)					
				Schlumberger–Wenner	Dipole–dipole	First electrode			Last electrode		
						X (m)	Y (m)	Z (m a.s.l.)	X (m)	Y (m)	Z (m a.s.l.)
1	53.0	1.0	5	2.5	6.8	457325	4688922	992	457323	4688870	994
2	108.0	1.5	5	3.2	14.3	457317	4688822	994	457420	4688819	1012
3	142.0	2.0	4	64.4	88.5	457336	4689079	998	457477	4688948	1014
4	142.0	2.0	3	32.1	39.6	457305	4689107	987	457333	4688970	990
5	142.0	2.0	3	60.2	67.0	457290	4689057	994	457306	4688975	1001
6	142.0	2.0	5	4.1	17.2	457256	4689035	992	457287	4688914	1000
7	142.0	2.0	4	56.6	56.4	457227	4689082	988	457241	4688941	990
8	142.0	2.0	5	7.5	19.0	457248	4689012	989	457369	4689052	1006
9	142.0	2.0	5	8.1	19.9	457248	4689012	989	457464	4689096	1012
10	142.0	2.0	5	2.6	5.9	457353	4689003	1007	457488	4690000	1038
11	106.0	2.0	3	44.9	56.8	457343	4689094	999	457399	4689178	1030
12	87.5	2.5	5	22.7	50.2	457307	4689132	1004	457372	4689177	1019
13	355.0	5.0	5	4.9	42.3	457482	4688736	1027	457280	4688442	1004
14	355.0	5.0	4	8.0	8.6	457190	4688603	998	457527	4688676	1016
15	355.0	5.0	5	3.2	23.2	457229	4688755	1004	457562	4688637	1017

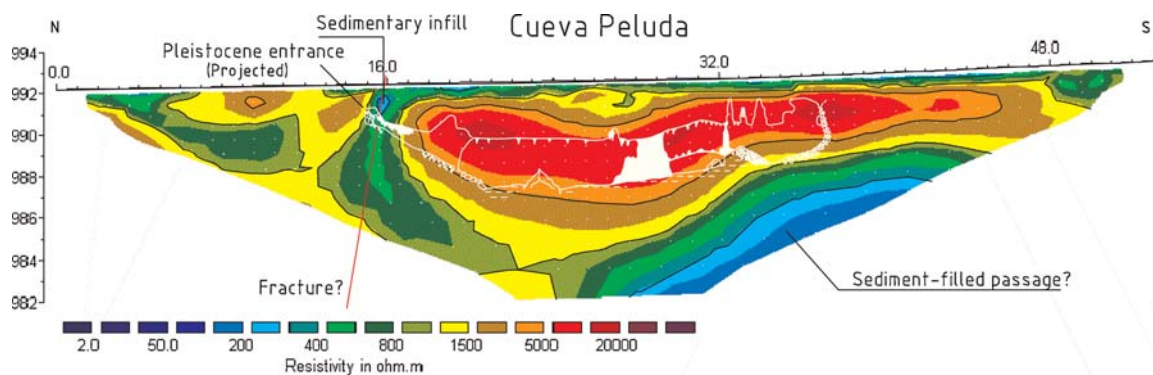


Figure 2. Electrical resistivity tomography profile recorded over Cueva Peluda karstic passage (profile 1). The white line shows the internal wall of the cave. This figure is available in colour online at wileyonlinelibrary.com.

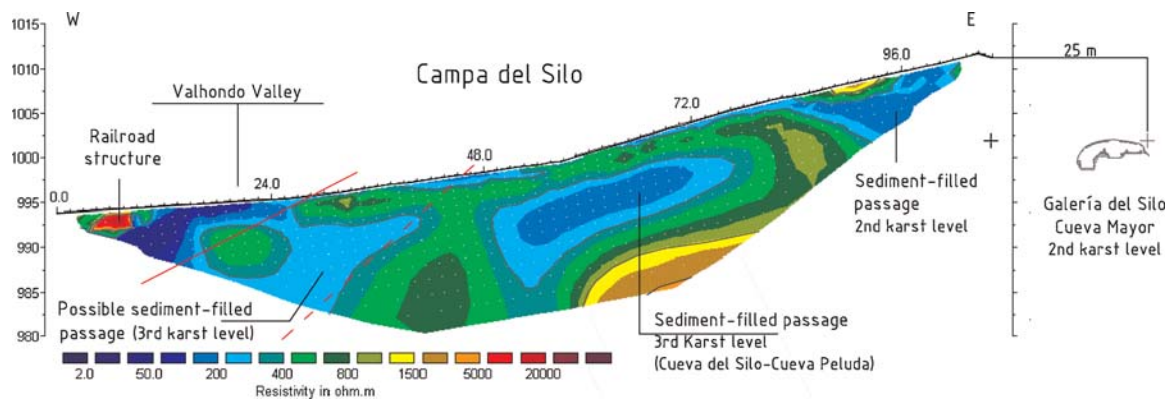


Figure 3. Electrical resistivity tomography profile recorded in the Valhondo valley, Campa del Silo (profile 2). See location in Figure 1C. This figure is available in colour online at wileyonlinelibrary.com.

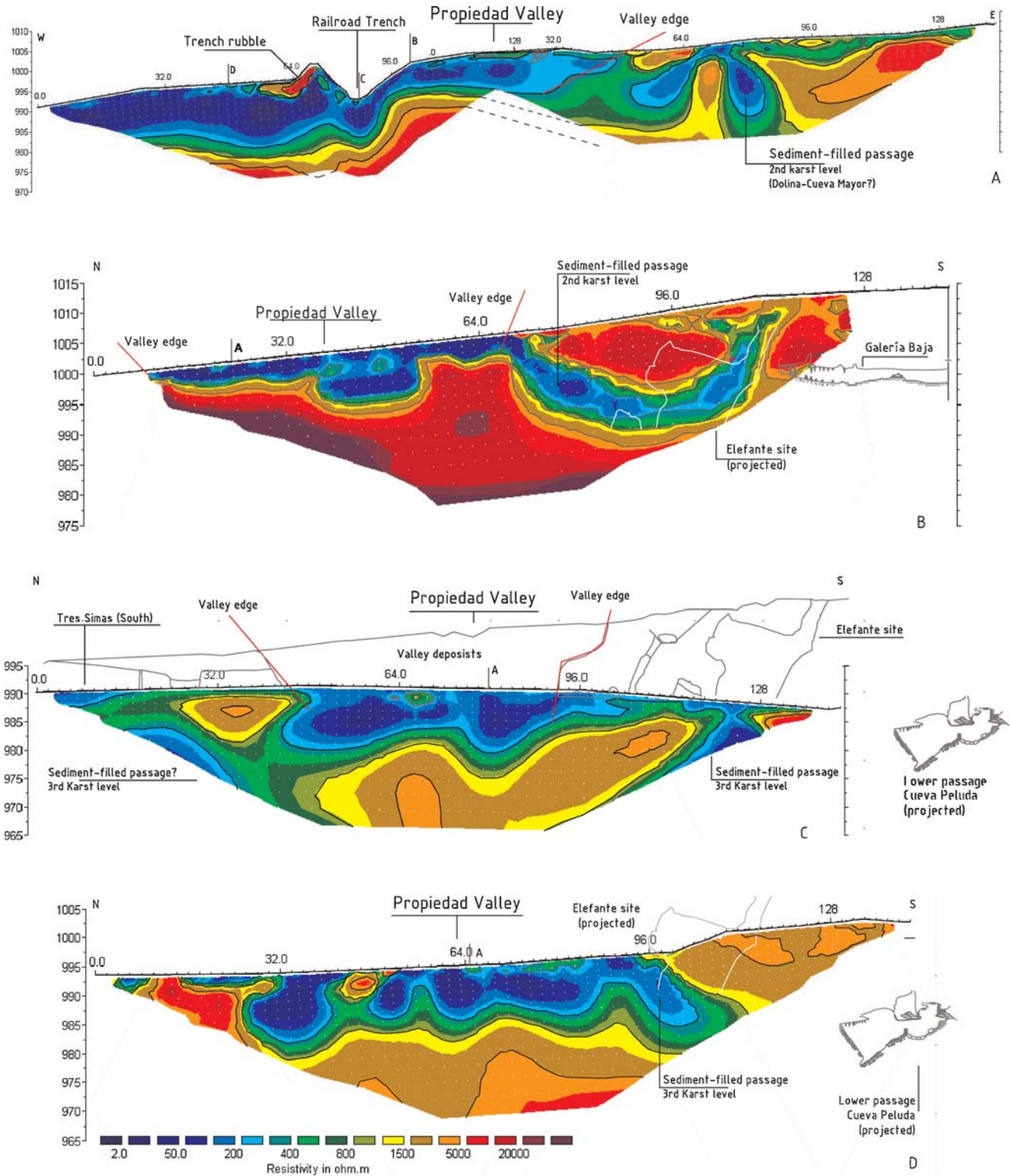


Figure 4. Electrical resistivity tomography profiles recorded in the Propiedad valley. (A) Longitudinal profile (number 9). (B–D) Transverse profiles (numbers 3–5). See location in Figure 1C. This figure is available in colour online at wileyonlinelibrary.com.

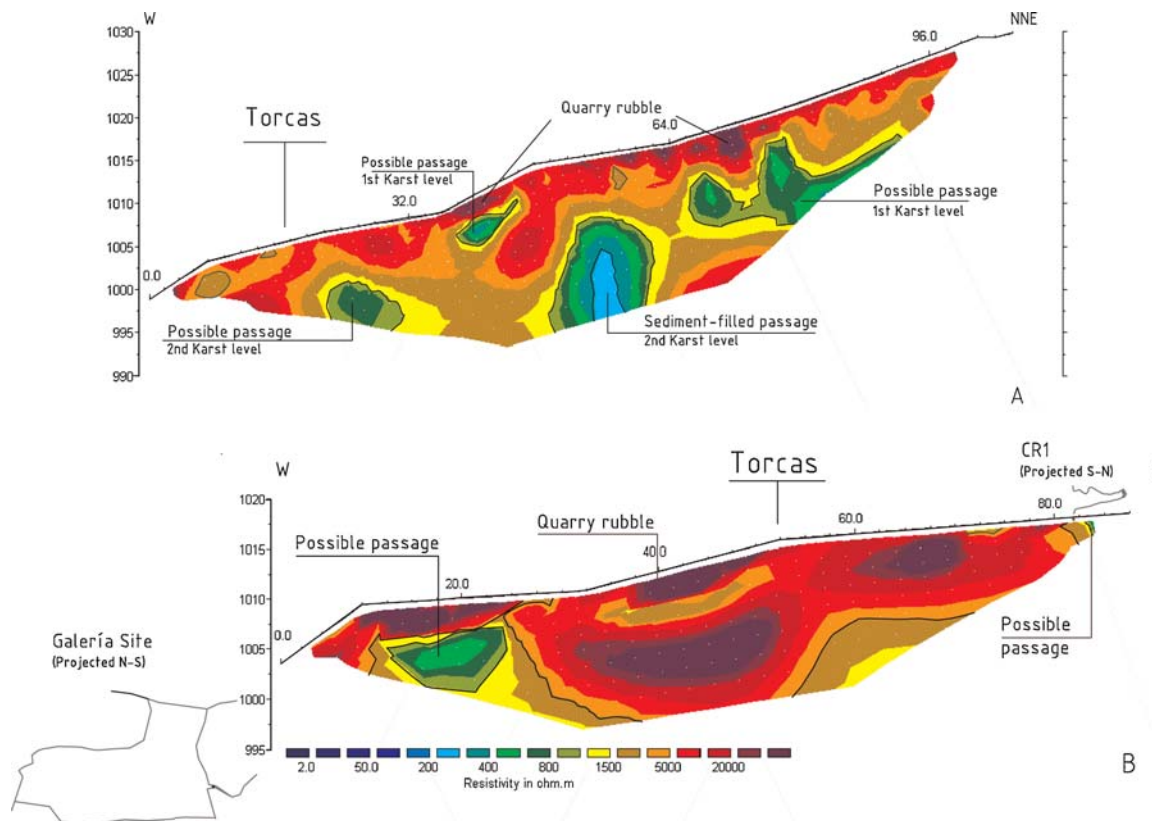


Figure 5. Electrical resistivity tomography profiles recorded in the Torcas Terrain, close to the Dolina and Galería archaeo-palaeoanthropological sites (profiles 11 and 12). See location in Figure 1C. This figure is available in colour online at wileyonlinelibrary.com.

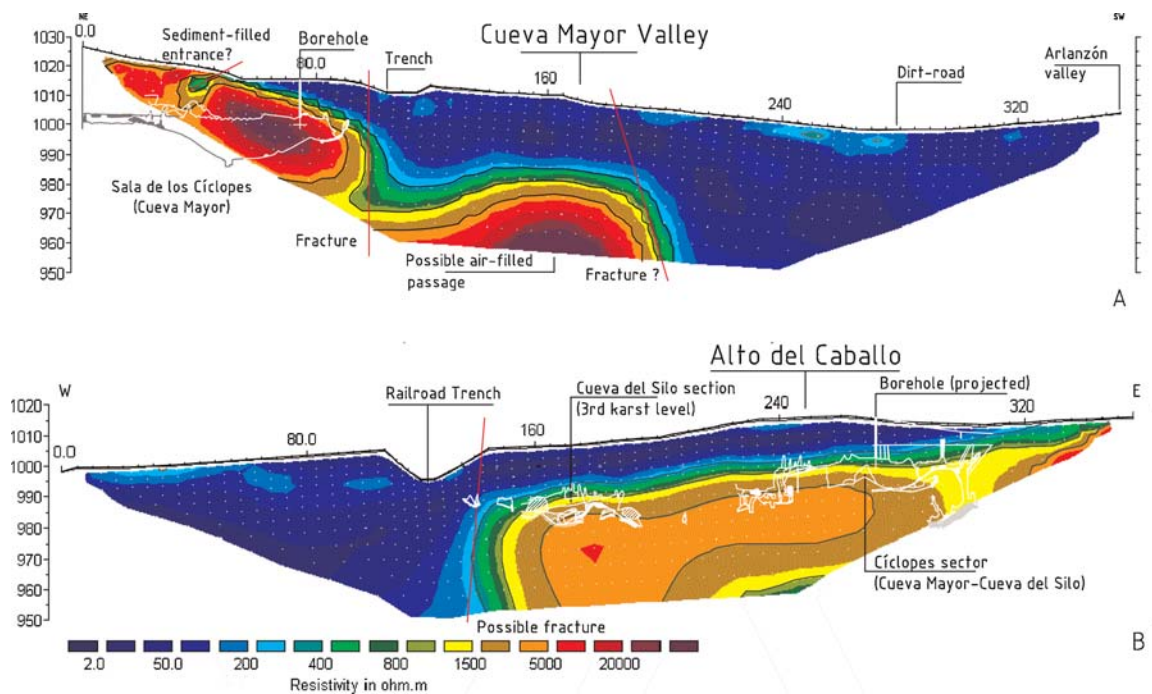


Figure 6. Electrical resistivity tomography profiles recorded in the Cueva Mayor valley (profiles 13 and 14). See location in Figure 1C. This figure is available in colour online at wileyonlinelibrary.com.

along the abandoned rail cutting above the well-known shallow main passage of the Peluda Cave and was used as a first control for the resistivity response of the cavities, sediments and materials. In this section, the dipole–dipole and Schlumberger–Wenner arrays show similar results. Profile 1 presents a closed structure denoted by the highest resistivity values ($> 1500 \text{ ohm m}^{-1}$, Figure 2), corresponding to the empty cavity of Cueva Peluda, barely a few metres (1–2 m) under the current floor of the railway cutting (*Trincheras*), between 992 and 990 m a.s.l. This structure is surrounded by rock (Upper Cretaceous carbonates), defined by a wide range of resistivities ($> 400 \text{ ohm m}^{-1}$), according to its degree of fracturing, local facies and stratification. In the profile, a third zone with the lowest resistivity values ($< 400 \text{ ohm m}^{-1}$) can be distinguished. The latter correspond to non-consolidated and higher porosity material, which correspond to a sediment-filled old entrance and passage, such as observed in several profiles recorded in the Valhondo and Propiedad valleys.

Valhondo valley

The Valhondo valley is located between Propiedad and Cueva Mayor valleys, and corresponds to a smooth valley that drains into the Pico River (Figures 1C.2 and 3). In this area, Cueva del Silo and Cueva Peluda develop at about 995–980 m a.s.l. (third endokarstic level), both containing metamorphic fluvial gravels, which are located at the same morphological level (985–983 m a.s.l.). The aim of the ERT prospection was to check the connection between these passages, whose formation and extension is a key aspect in understanding the post-depositional processes at the Elefante site (Rosas *et al.*, 2006; Ortega, 2009). The latter would explain the distribution of the gravels in the two cavities due to a single influx from the Arlanzón fluvial system to the endokarst during Early–Middle Pleistocene times.

In Valhondo valley profile, we distinguish the contact between the Upper Cretaceous carbonates to the east and the Neogene sediments to the west (Figure 3). In the Neogene sediments a high resistivity zone appears, which coincides with ballast corresponding to the old railway and the present road. However, in the Upper Cretaceous sediments three low resistivity zones were detected at different levels. The higher is located to the east at 1010 m a.s.l., being interpreted as a filled passage open to the outside at two sectors. This passage is located in the second endokarstic level in a position close to Galería Baja. The

other two low resistivity structures present a position similar to the third endokarstic level (996–990 m a.s.l.) and were interpreted as filled passages developed between Cueva Peluda and Galería del Silo. One of them presents a close oval morphology, while the other is opened to the sediments of Valhondo valley (see Figure 7) like the passages detected in Propiedad valley.

Propiedad valley

This valley drains the south flank of the Sierra de Atapuerca, from the upper plateau to converge with the Valhondo and Pico valleys in the Neogene Basin (Figure 1C.3–9), where Quaternary alluvial and colluvial sediments crop out.

The Elefante archaeo-palaeoanthropological site of Early–Middle Pleistocene age (Rosas *et al.*, 2006; Carbonell *et al.*, 2008), developed in the southern margin of this valley. Lower stratigraphical units of the Elefante site (Phase I, TE9–14; Rosas *et al.*, 2001), which contain human fossils of 1.1–1.2 Ma, show deformational structures and are affected by erosional processes. The upper units are characterized by significant water current deposits (Phase II, TE15–19; Rosas *et al.*, 2001). Drilling carried out in the base of the Elefante site showed quartzite gravels at –8 m (Rosas *et al.*, 2001).

Five transverse and two longitudinal ERT profiles were carried out at the Elefante site and the Propiedad valley in order to estimate the geometry of the sedimentary infill and the bedrock, which could explain the deformational processes and the presence of allochthonous sediments in this cavity. The results of these profiles (Figure 1C.3–9) are shown in Figure 4.

In the upper reach (Figures 1C.8 and 4A), the valley bottom develops on Upper Cretaceous limestones and dolostones characterized by high resistivity values (400–5000 ohm m). However, circular shaped anomalies were described in the carbonate rocks (Figure 4A; profile 8, Figure 1C), denoted by the lowest resistivity values ($< 400 \text{ ohm m}^{-1}$), or medium resistivity values (400–800 ohm m⁻¹). The shape and development level has made it possible to interpret these anomalies as karstic passages belonging to the second level of the endokarst system (1000–1010 m a.s.l.), filled by non-consolidated sediments (lower resistivity values) and probably by consolidated speleothems common in the nearest known passages (medium resistivity values; Figure 4A). The correspondence between the lowest resistivity values and the non-consolidated sediments were checked downstream, where the valley contains a Pleistocene sedimentary infill with resistivities lower than

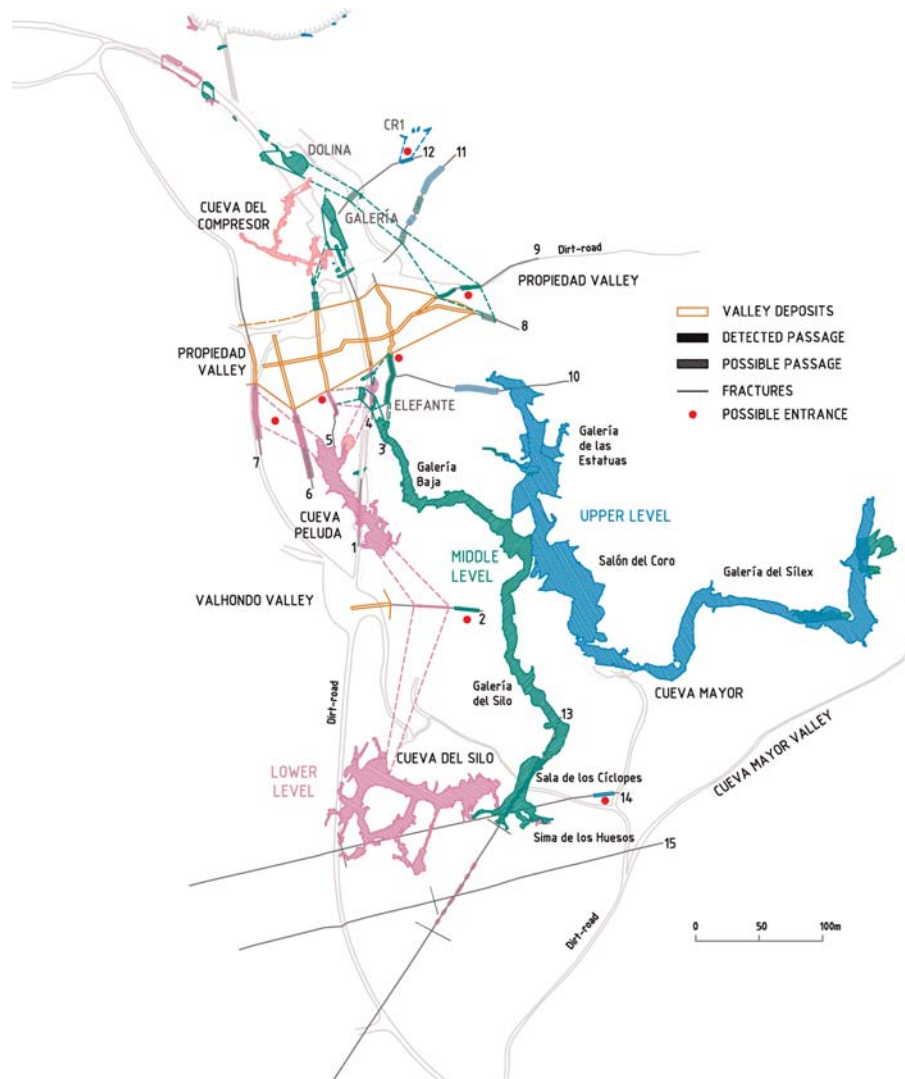


Figure 7. Electrical resistivity tomography interpretation superimposed on the projection of the multilevel karst of Sierra de Atapuerca on the ground surface. This figure is available in colour online at wileyonlinelibrary.com.

400 ohm m^{-1} . In the same way, in a transverse profile carried out in this area (Figure 4B), a filled karstic passage continuation of the Galería Baja (second endokarstic level) appears open to the valley sedimentary infill. This passage developed in a close position to the Elefante site, which is located at the end of Galería Baja (Figure 1C.3), suggesting that the sedimentary infill at Elefante could contain allochthonous alluvial⁻¹colluvial sediments derived from the valley through this kind of passage, such as the reworked marls and the fluvial facies observed in TE15–17 (Benito-Calvo and Pérez-González, 2007; Ortega, 2009). At the same level, this passage develops an elongated and almost closed pool in the valley bedrock. This geomorphological data indicates that the

structure would correspond to a phreatic cavity belonging to the second endokarstic level, captured by the valley and filled by sediments ($< 400 \text{ ohm m}^{-1}$). The presence of the filled and captured karstic cavities that were detected in the Propiedad valley supports the connection between Cueva Mayor–Cueva del Silo system and the Galería–Dolina cavities (Figures 1C and 7), associated with the first and second levels of the Sierra de Atapuerca endokarst system.

In the area of the Trincheras site (Figure 1C.4), the Propiedad valley sedimentary infill is exposed in a section composed of marls, sands, clays and carbonate gravels, organized in several units separated by disconformities (Benito, 2004). The ERT profiles carried out in this area show that these sediments

present low resistivity values, which extend vertically until 980–983 m a.s.l. (Figure 4C). This interpretation indicates that the sedimentary infill in this area presents a total thickness of 20–24 m, while other Sierra de Atapuerca minor valleys have no sediments or present only superficial deposits (Benito-Calvo *et al.*, 2008). The bedrock valley under this thick sedimentary infill describes a well-marked break in the bedrock longitudinal profile and semicircular depressions at the bottom (Figure 4A–C). The base of these depressions developed at the same level as the passages of the third endokarstic level, such as Cueva Peluda or the cavity detected under Elefante (Figures 1C.5 and 4C). The presence of this cavity would explain the deformation of the Elefante lower stratigraphical units and the presence of quartzite gravels under the Elefante infill. The cavity located under the Elefante site belongs to the third endokarstic level, where quartzite gravels and pebbles derived from Arlanzón River have been described. Collapse of the roof in this cavity would have caused the deformation of the Elefante infill.

The morphology of the bedrock valley suggest that these depressions are karstic and belong to the third endokarstic level, which were captured by the incision of the Propiedad valley. The depressions generated by the capture of these cavities would have facilitated the sedimentation of a thick sequence during rising base level, related to a subsequent regional phase of fluvial aggradation.

Downstream of Trinchera the bedrock morphology also suggests that the valley captured previous cavities of the third endokarstic level (Figure 4D). The carbonates that constitute the bedrock of the valley preserve marked semicircular depressions, currently filled with low resistivity materials corresponding to allochthonous sediments. At the same level of these bedrock morphologies and in the southern margin of the Propiedad valley (Figures 4 and 7), another low resistivity structure preserved in the carbonate rocks was detected. The structure has an elongated morphology and it is open to the valley sediments, being interpreted as a filled karstic passage continuation of Cueva Peluda. These passages could have worked as palaeo-springs during the Early–Middle Pleistocene, when the phreatic levels were higher.

Torcas Terrain

The Torcas Terrain is situated to the north of Propiedad valley (Figures 1C.11 and 12), in the area where the Early and Middle Pleistocene sites of Dolina and Galería are located (Bermúdez de Castro

et al., 1997; Carbonell *et al.*, 1999). These archaeo-palaeoanthropological sites are old entrances to the caves, which were filled by allochthonous sediments during the Pleistocene (Pérez-González *et al.*, 2001). Currently these sediments are exposed by a railroad cutting (*Trinchera*). In this area, the aim of ERT prospecting was to characterize the development and continuation of the karstic passages in order to check the continuation of the Dolina and Galería sites. The profiles indicate high resistivity values ($> 3000 \text{ ohm m}^{-1}$) corresponding to the Upper Cretaceous carbonates and to rubble accumulated from mining activities during the thirteenth century (Figures 1C.12 and 5). In addition, other closed structures inside the Upper Carbonates, denoted by medium resistivity values ($400\text{--}1000 \text{ ohm m}^{-1}$), could be distinguished. These were interpreted as small karstic cavities, in some cases probably filled with consolidated speleothems (Figure 5A and 5B). The lowest resistivity values detected are related to a large, closed structure (200 ohm m^{-1}), corresponding to a passage containing detrital sediment. All these passages generally develop at the same position of the second endokarstic level, representing the continuation of the Dolina and Galería cavities (Figure 5). The latter probably would be associated with a transitional level in this area between the first (Galería de las Estatuas) and second (Dolina cavity) endokarstic levels (see Figure 7), probably related to the decrease in elevation caused by the proximity of the spring of the Torcas area (Ortega *et al.*, 2005).

Cueva Mayor valley

This valley developed from the Sierra de Atapuerca upper plateau to the Arlanzón valley, eroding first the Upper Cretaceous limestone and dolostones, and then the Miocene alluvial and lacustrine sediments of the Duero Basin. The cavities documented in this valley all develop in the northern margin, where the Cueva del Silo and Cueva Mayor systems are located. The latter contain important stratigraphic levels related to phreatic and vadose events, which are followed by an inactive phase associated with the formation of speleothems and the use of the cavities by humans and fauna (Arsuaga *et al.*, 1997; Bischoff *et al.*, 2006). The profiles were recorded in the northern margin of the valley (Figure 1C.13–15) with the aim of analysing the geological structure responsible of the passage distribution and also detecting other possible old entrances filled by sediments, which could explain the presence of bear and hominids in the Sima de los Huesos and Cíclopes room.

In order to detect cavities located at greater depths we had to increase the lengths and electrode spacing of the ERT profiles (Table 1). The geological structure interpreted in the area is characterized by a clear contact between the Upper Cretaceous carbonates (resistivities $>400 \text{ ohm m}^{-1}$) and the Miocene sediments (resistivities $<40 \text{ ohm m}^{-1}$) (Figures 1C.13 and 14, 6A and B). The contact between these geological units shows marked steps, which were interpreted as faults. The larger step was detected in two profiles under 985 m a.s.l., showing a fall greater than 35 m (Figure 6A and B). This fault puts the Upper Cretaceous carbonates in contact with the lower units of the Neogene sequence (Figure 6A), which in the area corresponds to marls, clays and evaporites of the Lower Miocene. Overlying these sediments, the Middle Miocene unit which crops out in *Trinchera* is affected by minor faults or appears filling a palaeorelief surface on the Upper Cretaceous carbonates (Figure 6A and B). This palaeorelief is characterized by a gradual slope of 89° from east to west (Figure 6B), similar to the 7° of dip of the Middle Miocene sediments in this flank of the Sierra de Atapuerca (Benito-Calvo *et al.*, 2008).

The greater length and gap between these profiles that was necessary to increase the depth of prospecting affects the resolution, preventing the detection of small passages and entrances. Only the larger cavities are reflected in these sorts of profiles, although with imprecise shape, such as the Sala de los Cíclopes with $16\,168 \text{ m}^3$ of air volume (Figures 1C.13, 6A and 7.13). However, the plotting of the karst topography on the ERT profiles has made it possible to confirm that the cavities developed in the Upper Cretaceous carbonates, close to the contact with the mainly impermeable Neogene sediments (Figure 6A and 6B), which prevent the karst development toward the left margin of the Cueva Mayor Valley. This contact usually takes place through faults very near to the Arlanzón valley, which could have played an important role in the karst hydrology (Figure 7).

Conclusions

Electrical resistivity tomography (ERT) has been a useful non-destructive geophysical method for imaging the subsurface structures of the south flank of the Sierra de Atapuerca and its endokarst system, whose entrances were occupied by Early and Middle Pleistocene hominids. The use of detailed geomorphological and geological maps of the endokarst system and the surface landscape was essential to

reduce the uncertainty of the geophysical interpretation. High resolution ERT prospecting made it possible to detect and analyse structures related to the site formation and distribution, such as bedrock morphologies, cavity continuity, geometries and thickness of sedimentary infills, and old entrances filled by sediments. Deeper prospecting, related to longer length and lower resolution sections, was suitable to analyse deeper geological structures that controlled the development of the endokarst.

The analysis of this information contributes important new data about the configuration and geodynamic evolution of this endokarst. The second and third endokarstic levels develop from these faults, close to the Arlanzón valley, toward the north and finish in the Pico valley. This third level was detected under Elefante, explaining the presence of fluvial facies under Elefante, and the collapse of the Elefante lower stratigraphical units. The geophysical prospecting thus allowed us to infer the connection between allegedly isolated cavity systems, such as between Cueva del Silo and Cueva Peluda (third level), or between the passages of Galería Baja-Elefante and Galería-Dolina (second level) (Figure 7). This development from south to north is cut off partially by the of Propiedad valley, whose Pleistocene incision captured cavities, forming entrances to the cavities that represent new potential sites. This work is fundamental for the understanding of the distribution of archaeological sites in the area and to plan their investigation.

Acknowledgements

This work was supported by the research projects BXX2000-1258-03-02, BOSS2003-08938-C03-01 and CGL2006-13532-C03-02 of the Dirección General de Investigación Científica y Técnica (DGICYT), and by the Junta de Castilla y León. The authors wish to thank the multidisciplinary research team of the Sierra de Atapuerca (EIA) and the Grupo Espeleológico Edelweiss for constant scientific and logistic support. The authors thank Professor Paul Goldberg for careful reading of the manuscript during its preparation. Rolf Quam revised the English in the final draft of the manuscript. The authors would like to thank two anonymous reviewers for their comments and critical review of the manuscript.

References

- Armenteros I, Corrochano A, Alonso-Gavilán G, Carbalreira J, Rodríguez JM. 2002. Duero Basin (northern

- Spain). In *Geology of Spain*, Gibbons W, Moreno T editors. Geological Society Publishing House: Bath; 309–315.
- Arsuaga JL, Martínez I, Gracia A, Carretero JM, Carbonell E. 1993. Three new human skulls from the Sima de los Huesos site in Sierra de Atapuerca, Spain. *Nature* **362**: 534–537.
- Arsuaga JL, Martínez I, Gracia A, Carretero JM, Lorenzo C, García N, Ortega AI. 1997. Sima de los Huesos (Sierra de Atapuerca, Spain). The site. *Journal of Human Evolution* **33**(2/3): 109–127.
- Astin T, Eckardt H, Hay S. 2007. Resistivity imaging survey of the Roman Barrows at Bartlow, Cambridgeshire, UK. *Archaeological Prospection* **14**: 24–37.
- Athanasiou EN, Tsourlos PI, Papazachos CB, Tsokas GN. 2007. Combined weighted inversion of electrical resistivity data arising from different array types. *Journal of Applied Geophysics* **62**: 124–140.
- Benech Ch, Hesse A. 2007. Some considerations on the integration of geophysical data into archaeological research. In *Geophysik aund Ausgrabung. Einsatz und Auswertung zerstörungsfreier Porspektion in der Archäologie*. Internationale Archäologie Naturwissenschaft und Technologie: 175–186.
- Benito A. 2004. *Análisis geomorfológico y reconstrucción de paleopaisajes neógenos y cuaternarios en la Sierra de Atapuerca y el valle medio del río Arlanzón*. PhD Tesis, Universidad Complutense, Madrid, Spain, 381 pp, ISBN 84-669-2585-6.
- Benito-Calvo A, Pérez-González A. 2007. Erosion surfaces and Neogene landscape evolution in the NE Duero Basin (north-central Spain). *Geomorphology* **88**: 226–241.
- Benito-Calvo A, Pérez-González A, Parés JP. 2008. Quantitative reconstruction of late Cenozoic landscapes: a case study in the Sierra de Atapuerca (Burgos, Spain). *Earth Surface Processes and Landforms* **33**: 196–208.
- Beresnev IA, Hruby C, Davis C. 2002. Exploration Geophysics. *Journal of Applied Geophysics* **49**: 245–254.
- Bermúdez de Castro JM, Arsuaga JL, Carbonell E, Rosas A, Martínez I, Mosquera M. 1997. A hominid from the Lower Pleistocene of Atapuerca, Spain: possible ancestor to Neandertals and modern human. *Science* **276**: 1392–1395.
- Bermúdez de Castro JM, Carbonell E, Arsuaga JL (eds). 1999. Gran Dolina Site: TD6 Aurora Stratum (Burgos, Spain). *Journal of Human Evolution* **37**(3/4): 309–700.
- Bischoff JL, Williams RW, Rosenbauer RJ, Aramburu A, Arsuaga JL, Gracia N, Cuenca-Bescós G. 2006. High-resolution U-series dates from the Sima de los Huesos hominids yields 600+infinito/– 66 kyrs: implications for the evolution of the early Neanderthal lineage. *Journal of Archaeological Science* **34**: 763–770.
- Carbonell E, Rosas A, Díez JC editors. 1999. *Atapuerca: Ocupaciones humanas y paleoecología del yacimiento de Galería*. *Arqueología en Castilla y León* 7. Junta de Castilla y León: Zamora; 390 pp.
- Carbonell E, Bermúdez de Castro JM, Parés JM, Pérez-González A, Cuenca-Bescós G, Ollé A, Mosquera M, Huguet R, Made Jvander, Rosas A, Sala R, Vallverdú J, García N, Granger DE, Martínón-Torres M, Rodríguez XP, Stock GM, Vergès JM, Allue E, Burjachs F, Cáceres I, Canals A, Benito A, Díez C, Lozano M, Mateos A, Navazo M, Rodríguez J, Rosell J, Asuaga JL. 2008. The first hominin of Europe. *Nature* **425**: 465–470.
- Cardarelli E, Di Filippo G. 2009. Integrated geophysical methods for the characterisation of an archaeological site (Massenzio Basilica – Roman forum, Rome, Italy). *Journal of Applied Geophysics* **68**: 508–521.
- Chambers JE, Ogilvy RD, Kuras O, Cripps JC, Meldrum PL. 2002. 3D electrical imaging of known targets: a controlled environmental test site. *Environmental Geology* **41**: 690–704.
- Dahlin T. 2001. The development of DC resistivity imaging techniques. *Computer and Geosciences* **27**: 1019–1029.
- Daily W, Ramirez AL. 2000. Electrical imaging of engineered hydraulic barriers. *Geophysics* **65**: 83–94.
- Drahor MG, Berge MA, Kurtulmus TÖ, Hartmann M, Speidel MA. 2008. Magnetic and electrical resistivity tomography investigations in a Roman legionary camp site (Legio IV Scythica) in Zeugma, Southeastern Anatolia, Turkey. *Archaeological Prospection* **15**: 159–186.
- Eraso A, Domínguez MC, Ortega AI, Martín-Merino MM, Pérez-González A. 2001. Estimación de las paleovelocidades y sentidos de circulación del agua en el karst donde se emplaza el yacimiento arqueológico de la Sierra de Atapuerca (Burgos). *Boletín de la Sociedad Española de Espeleología y Ciencias del Karst* **2**: 61–68.
- Ford DC. 1977. Genetic classification of solutional cave systems. *Proceedings of the 7th International Congress of Speleology*, Sheffield; 189–192.
- Griffiths DH, Turnbull J, Olayinka AI. 1990. Two-dimensional resistivity mapping with a computer-controlled array. *First Break* **8**: 121–129.
- Griffiths DH, Barker RD. 1993. Two-dimensional resistivity imaging and modelling in areas of complex geology. *Journal of Applied Geophysics* **29**: 211–226.
- Griffiths DH, Barker RD. 1994. Electrical Imaging in Archaeology. *Journal of Archaeological Science* **21**: 153–158.
- Klimchouk A. 2009. Morphogenesis of hypogenic caves. *Geomorphology* **106**: 100–117.
- Loke MH. 1999. RES2DINV ver. 3.42, Geoelectrical Imaging 2D & 3D, User Manual.
- Loke MH, Barker RD. 1996. Rapid least-squares inversion of apparent resistivity pseudosections using a quasi-Newton method. *Geophysical Prospecting* **44**: 131–152.
- Loke MH, Dahlin T. 2002. A comparison of the Gauss-Newton and Quasi-Newton methods in resistivity imaging inversion. *Journal of Applied Geophysics* **49**: 149–162.
- Maillol JM, Seguin M-K, Gupta OP, Akhauri HM, Sen N. 1999. Electrical resistivity tomography survey for delineating uncharted mine galleries in West Bengal, India. *Geophysical Prospecting* **47**: 103–116.
- Martín MA, Domingo Mena S, Antón Palacios T. 1981. Estudio de las cavidades de la zona BU-IV-A (Sierra de Atapuerca). *Kaite, Estudios de Espeleología Burgalesa* **2**: 41–76.
- Ortega AI. 2009. Evolución geomorfológica del Karst de la Sierra de Atapuerca (Burgos) y su relación con los yacimientos pleistocenos que contiene. Unpublished PhD Thesis, Universidad de Burgos, Burgos, Spain, 624 pp. I Annex Planimetric Documentation (11 maps, 12 long-sections, 91 cross-sections).

- Ortega AI, Pérez-González A, Martín MA, Carretero JM, Arsuaga JL. 2005. El Sistema de Cueva Mayor-Cueva del Silo. Un estudio Morfológico del Endokarst de la Sierra de Atapuerca (Burgos, España). In *Geoarqueología y Patrimonio en la Península Ibérica y el entorno Mediterráneo*, Santonja M A, Pérez-González A editors. ADEMA: Soria; 161–179.
- Palmer AN. 1991. Origin and morphology of limestone caves. *Geological Society of America Bulletin* **103**: 1–21.
- Papadopoulos NG, Tsourlos P, Tsokas GN, Sarris A. 2006. Two-dimensional and three-dimensional electrical imaging in archaeological site investigation. *Archaeological Prospection* **13**: 163–181.
- Papadopoulos NG, Yi M-J, Kim J-H, Tsourlos P, Tsokas GN. 2010. Geophysical investigation of tumuli by means of surface 3D electrical resistivity tomography. *Journal of Applied Geophysics* **70**: 192–205.
- Parés JM, Pérez-González A. 1995. Paleomagnetic age for hominid fossils at Atapuerca archaeological site, Spain. *Science* **269**: 830–832.
- Parés JM, Pérez-González A, Rosas A, Benito A, Bermúdez de Castro JM, Carbonell E, Huguet R. 2006. Matuyama-age lithic tools from the Sima del Elefante site, Atapuerca (northern Spain). *Journal of Human Evolution* **50**: 163–169.
- Pérez-González A, Parés JM, Carbonell E, Aleixandre T, Ortega AI, Benito A, Martín-Merino MA. 2001. Géologie de la Sierra de Atapuerca et stratigraphie des remplissages karstiques de Galería et Dolina (Burgos Espagne). *L'Anthropologie* **105**(1): 27–44.
- Pineda A. 1997. *Mapa Geológico de España escala 1:50.000, 2ª Serie (MAGNA)*. Hoja de Burgos, 200 (19-10). IGME, Madrid, 93 pp.
- Piro S, Mauriello P, Cammarano F. 2000. Quantitative integration of geophysical methods for archaeological prospection. *Archaeological Prospection* **7**: 203–213.
- Piro S, Tsourlos P, Tsokas GN. 2001. Cavity detection employing advanced geophysical techniques: a case study. *European Journal of Environmental and Engineering Geophysics* **6**: 3–31.
- Porres JA. 2003. *Caracterización de cavidades en el subsuelo mediante la interpretación de perfiles de Tomografía Eléctrica*. PhD thesis, Universidad de Burgos, Burgos, Spain; 343–346. ISBN: 9788496394551.
- Rosas A, Pérez González A, Carbonell E, Made Jvander, Sánchez A, Laplana C, Cuenca-Bescós G, Parés JM, Huguet R. 2001. Le gisement pléistocène de la 'Sima del Elefante' (Sierra de Atapuerca, Espagne). *L'anthropologie* **105**: 301–312.
- Rosas A, Huguet R, Pérez-González A, Carbonell E, Bermúdez de Castro JM, Vallverdú J, van der Made J, Allué E, García N, Martínez-Pérez R, Rodríguez J, Sala R, Saladie P, Benito A, Martínez-Maza C, Bastir M, Sánchez A, Parés JM. 2006. The 'Sima del Elefante' cave site at Atapuerca (Spain). *Estudios Geológicos* **62**: 327–348.
- Tsokas GN, Tsourlos PI, Stampolidis A, Katsonopoulou D, Soter S. 2009. Tracing a major Roman road in the area of ancient Helike by resistivity tomography. *Archaeological Prospection* **16**: 251–266.